

Observation of dynamical phase transitions in a topological nanomechanical system

Tian Tian^{1,2}, Yongguan Ke^{3,6}, Liang Zhang^{1,2}, Shaochun Lin^{1,2}, Zhifu Shi^{1,2,4}, Pu Huang⁵,
Chaohong Lee^{3,6,*} & Jiangfeng Du^{1,2,4,*}

¹CAS Key Laboratory of Microscale Magnetic Resonance and Department of Modern Physics, University of Science and Technology of China, Hefei 230026, China

²Synergetic Innovation Center of Quantum Information and Quantum Physics, University of Science and Technology of China, Hefei 230026, China

³Laboratory of Quantum Engineering and Quantum Metrology, School of Physics and Astronomy, Sun Yat-Sen University (Zhuhai Campus), Zhuhai 519082, China

⁴Hefei National Laboratory for Physical Sciences at the Microscale, University of Science and Technology of China, Hefei 230026, China

⁵National Laboratory of Solid State Microstructures and Department of Physics, Nanjing University, Nanjing, 210093, China

⁶State Key Laboratory of Optoelectronic Materials and Technologies, Sun Yat-Sen University (Guangzhou Campus), Guangzhou 510275, China

Dynamical phase transitions, characterized by non-analytic behaviors in time domain, extend the equilibrium phase transitions to far-from-equilibrium situations ^{1,2}. Furthermore, it's predicted that the dynamical phase transitions can be precisely identified by discontinuities of Pancharatnam geometric phase during the time evolution, even in a general non-adiabatic and non-cyclic process ³⁻⁵. Here, we report the observation of dynamical phase transitions via directly measuring Pancharatnam geometric phase in a quenched topological nanomechanical system. We present a flexible strategy based on eight strong-coupled high-quality-factor nanomechanical oscillators to realize an one-dimensional reconfigurable lattice described by the Su-Schrieffer-Heeger Hamiltonian. Due to the chiral symmetry, the dynamical phase of the time-evolved state quenching from an initial topological edge state is

naturally eliminated, so that we can directly read the Pancharatnam geometric phase of the state. We find that, the Pancharatnam geometric phase jumps π when a dynamical phase transition takes place, which is detected by the normalized amplitude of edge oscillator. This work not only provides a quantitative method to identify the dynamical phase transitions, but also opens the door for studying non-equilibrium topological dynamics with a well-controlled nanomechanical system.

In recent years, non-equilibrium phenomena beyond the Ginzburg-Landau paradigm have attracted tremendous attentions and interests ^{1,2,5-18}. In analog to equilibrium phase transitions, dynamical phase transitions (DPTs) are a kind of outstanding non-equilibrium phenomena which manifest non-analytic behaviors of the rate function (i.e. the logarithm function of returning probability to initial state) in the time domain ^{1,2}. So far, DPTs in sudden quenches have been found by measuring the rate function or observing the dynamical vortices etc ¹³⁻¹⁶. Theoretically, in a DPT, the non-analytic behavior occurs and the Pancharatnam geometric phase (PGP) simultaneously jumps π at the critical time when the returning probability goes through zero ⁵. This means that the PGP provides an exact quantitative hallmark of DPTs. To the best of our knowledge, as the PGP in a quenched system always accompanies and mixes with the dynamical phase ^{2,5,16,18}, there is still no experiment observation of DPTs by directly measuring PGP.

We present a novel scheme for eliminating the dynamical phase in sudden quenches from a topological edge state, which is a prominent signature of nontrivial topology ¹⁹⁻²³. Considering the Su-Schrieffer-Heeger (SSH) model - a typical topological model ²⁴, due to its chiral symmetry ²⁵, the initial edge state equally populates all symmetrical pairs of final eigenstates and so that the dynamical phase is naturally eliminated. The scheme is different from the previous studies that quenching from the ground state ^{1,13-15} or a bulk state ^{5,16-18,26}.

To investigate the topological dynamics, we developed a method to fabricate the high-quality-factor nanomechanical array of eight oscillators with strong couplings. The quality factor can reach about 1×10^5 in vacuum at 77K temperature, which is further better than the previous

mechanical lattice at 4K temperature ²⁷. In this Letter, we report an experimental observation of DPTs via directly measuring PGP in this nanomechanical lattice. The coupled oscillators can be flexibly engineered by capacitive coupling ²⁸. Sudden quenches between different structures are easily configured by tuning the different coupling voltages between oscillators. The initial state preparation and high-resolution measurement are enable with the standard magneto-motive technique ²⁹. Since the dynamical phase is naturally eliminated, we directly observe the PGP and its jumps at critical times by demodulating the motion of the edge oscillator. We also observe the non-analytic behaviors of the rate function, which provides another signature of the DPTs. This is the first time exploring the relation between PGP and DPTs in experiment.

We study the quench dynamics in a one-dimensional (1D) topological model -the SSH chain ²⁴. This model describes a 1D super-lattice with two sites per unit cell, and its Hamiltonian reads

$$\hat{H} = J_A \sum_{j=odd} |j\rangle\langle j+1| + J_B \sum_{j=even} |j\rangle\langle j+1| + h.c. \quad (1)$$

where $|j\rangle$ is the state of exciting the j -th site, J_A and J_B are intracell and intercell hopping respectively showed in the top of Fig. 1a. Its topological aspects can be characterized by a topological invariant - the winding number ²⁵. In momentum space, the Hamiltonian is given as $\hat{H}(k) = \mathbf{d}(\mathbf{k}) \cdot \boldsymbol{\sigma}$ with the Pauli matrices $\boldsymbol{\sigma}$. The trajectory of $\mathbf{d}(\mathbf{k})$ does not encircle the origin point when $J_A > J_B$, so the winding number is $\mathcal{W} = 0$ and the structure is topological trivial. On the conversely, the winding number is $\mathcal{W} = 1$ and the structure is topological nontrivial when $J_A < J_B$, see Fig. 1b. According to bulk-edge correspondence, there exist topological edge states under open boundary condition if the bulk invariant is topological nontrivial. Under this condition, the energy spectra of two typical phases are different, which are showed in Fig. 2a (trivial phase) and Fig. 2c (nontrivial phase). There exist topological edge states (which appear as zero modes) in the band gap of topological nontrivial phase. Thus, we can distinguish topological trivial and nontrivial structures by the winding number or the existence of edge states.

We configure the 1D tight-binding model by a reconfigurable array in experiment, see Fig. 1a.

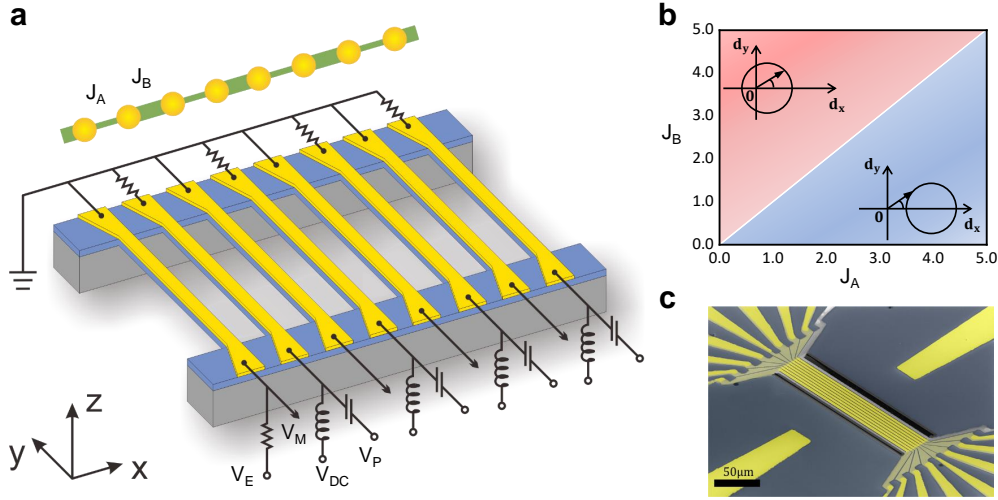


Figure 1: **Nanomechanical oscillators for simulating SSH model.** **a**, The sample of eight almost identical nanomechanical oscillators (doubly clamped beams) is fabricated by 100nm thick silicon nitride (dark blue) coat with a thin layer of gold. For every oscillator, the first mode of vibration (along z axis) is used in this work. The nearest-neighbor parametric couplings are realized by applying sum of V_{DC} and V_{AC} between every two adjacent oscillators. The unit cell of SSH chain is represented by two adjacent oscillators. The hopping strength (green lines) of SSH can be tuned by parametric couplings. Magnetic field is applied along x axis for excitation (V_E) and detection (black arrows). **b**, Equilibrium phase diagram of SSH model. If intracell hopping J_A is larger than intercell hopping J_B , SSH chain is trivial and the winding number $\mathcal{W} = 0$. Otherwise, the SSH chain is topological and the winding number $\mathcal{W} = 1$. **c**, False-color scanning electron micrograph of the sample.

The array consists of eight almost identical oscillators (doubly clamped beams). Every unit cell of SSH model includes two adjacent oscillators. The intracell and intercell hopping strengths are controlled by different nearest-neighboring parametric couplings, which are realized by applying voltage $V_{DC} + V_{AC}$ between two oscillators. The classical motion equations of coupled oscillators can be fully mapped onto the Hamiltonian of SSH model (see Methods). We choose 20Hz and 60Hz coupling strength alternately to realize a topological phase in SSH model. On the contrary, we realize a trivial phase by choosing 60Hz and 20Hz alternately. These two structures are determined by measuring the stabilized frequency response of the edge oscillator (see Methods).

We study the quench dynamics of a edge state from $\hat{H}_i : J_A/J_B \rightarrow 0$ to (i) $\hat{H}_{f1} : J_A > J_B$ and (ii) $\hat{H}_{f2} : J_A < J_B$. The initial state is prepared at the edge site, $|\psi(0)\rangle = (1, 0, \dots, 0)^T$, which is the eigenstate of a large dimeric topological Hamiltonian \hat{H}_i . The first quench cross the underlying topological phase transition, while the second quench stays in the same topological phase. The evolution of system follows $|\psi(t)\rangle = e^{-i\hat{H}_f t}|\psi(0)\rangle$ after quenches. The Loschmidt amplitude is given as

$$\mathcal{G}(t) = \langle \psi(0) | \psi(t) \rangle = r(t) e^{i\phi(t)} = \sum_n \mathcal{G}_n(t) \quad (2)$$

where $r(t)$ is the modulus of Loschmidt amplitude, $\phi(t)$ is the phase containing a dynamical phase $\phi^{dyn}(t) = -\int_0^t \langle \psi(s) | \hat{H}_f | \psi(s) \rangle ds$ and a PGP ϕ^P ⁵, and $\mathcal{G}_n(t) = |\langle \psi_n | \psi(0) \rangle|^2 e^{-iE_n t}$ is partial Loschmidt amplitude with eigenstates $|\psi_n\rangle$ and eigenvalues E_n of the final Hamiltonian \hat{H}_f .

Due to the chiral symmetry, the initial edge state equally populates all symmetrical pairs of final eigenstates so that the occupation $|\langle \psi_{-m} | \psi(0) \rangle|^2 = |\langle \psi_{+m} | \psi(0) \rangle|^2$, $m = 1, 2, 3, 4$ for the SSH chain. The occupations are showed in Fig. 2a and c. And the Fig. 2b and d show that, there is always symmetrical part for \mathcal{G}_n at each moment because of $E_{-m} = -E_{+m}$. Thus, Loschmidt amplitude $\mathcal{G}(t) \in \mathbf{R}$ and the phase $\phi(t)$ of Loschmidt amplitude is 0 or π all the time.

By the same reason, the dynamical phase keeps zero

$$\phi^{dyn}(t) = -\sum_n |\langle \psi_n | \psi(0) \rangle|^2 E_n t = 0 \quad (3)$$

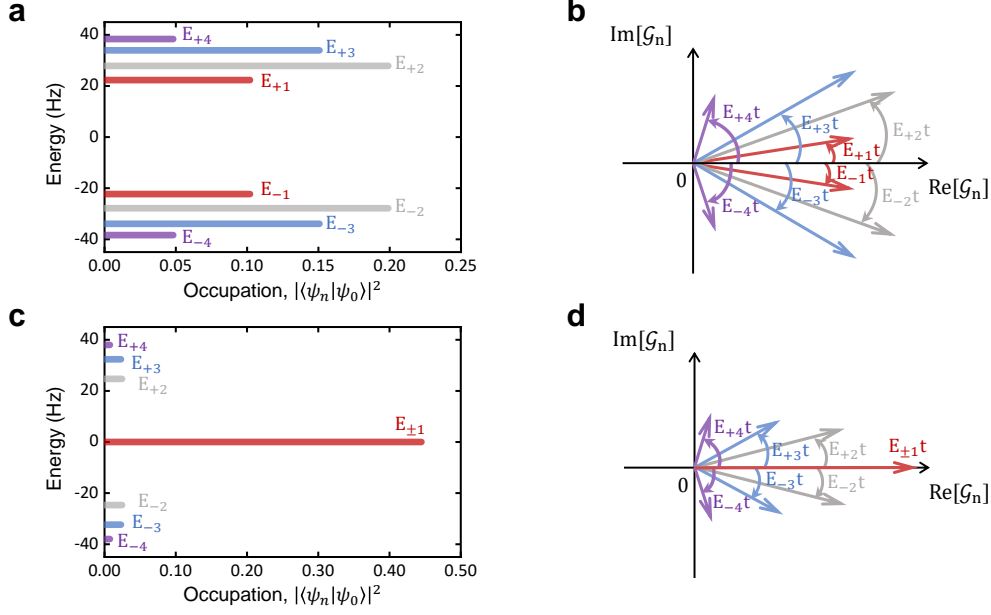


Figure 2: **Symmetric energy spectrum and partial Loschmidt amplitudes.** **a**, The energy spectrum of finial trivial SSH Hamiltonian and occupations of the initial edge state in finial eigenstates. **b**, The partial Loschmidt amplitude after sudden quench of edge state evolving under a trivial SSH Hamiltonian. **c**, The energy spectrum of finial topological SSH Hamiltonian and occupations of the initial edge state in finial eigenstates. **d**, The partial Loschmidt amplitude after sudden quench of edge state evolving under a nontrivial SSH Hamiltonian.

so that ϕ^{dyn} is naturally eliminated and the phase $\phi(t)$ we measure is directly give the PGP (see Supplementary Information). According to the original definition of DPTs ^{1,2}, the rate function derived from Loschmidt amplitude as

$$\lambda(t) = -\frac{1}{N} \ln |\mathcal{G}(t)|^2 = -\frac{1}{N} \ln |r(t)|^2 \quad (4)$$

will become nonanalytic at the critical time when DPTs take place. Thus, when Loschmidt amplitude $\mathcal{G}(t)$ goes through zeros in quenched dynamics, the DPTs take place while the PGP jumps π ⁵.

In experiment, quenches of topological edge state in different topological phases are realized by the different pulse sequences (see Supplementary Information). The preparation initial edge

state is applying a sinusoidal wave generated by AWG with ω_E to the first oscillator. At time $t = 0$, we turn on all the coupling voltages between every two adjacent oscillators to realize SSH Hamiltonian \hat{H}_f . As the time evolves, we measure the vibration of each oscillator with the lock-in amplifier. The measured signal is amplified and demodulated by a reference (generated by AWG). Both the vibrational amplitude and the phase can be extracted from lock-in phase-sensitive detection.

The Loschmidt amplitude and the PGP are obtained by the normalized amplitude and the vibration phase of the edge oscillator, respectively. In the quench-(i) (showed in Fig. 3a by red arrow) where the topological edge state evolves under the trivial Hamiltonian \hat{H}_{f1} that coupling strengths are 60Hz and 20Hz alternately, we observe the PGP jumps twice in 40ms evolution from Fig. 3b. In the quench-(ii) (showed in Fig. 3a by blue arrow) where the topological edge state evolves under the topological Hamiltonian \hat{H}_{f2} that coupling strengths are 20Hz and 60Hz alternately, we observe the PGP keeps unchanged in 40ms evolution from Fig. 3b. The initial nonzero PGP results from the external electric circuits, and it does not affect the jump behavior. The experimental results (circles and triangles) in Fig. 3b are measured by averaging 500 times, and they are in great agreement with the theoretical results.

To diagnose the DPTs, we also measure the rate function in these two quenches. We assume that all oscillators have the same decay rates in the short time of evolution, due to the strong coupling strengths much larger than the decay rates, the high quality factors and the small differences between the oscillators. Therefore, all amplitudes can be normalized every moment. We obtain the rate function from the normalized amplitude of the first oscillator in two quenches, and observe non-analytic behaviors of the rate function when the system is quenched across an underlying topological phase transition, see the red circles with error bar in the Fig. 3c. The non-analytic behaviors directly verify the DPTs. For the quench in the same topological phase, the rate function is always analytic, which suggests that there is no appearance of DPTs, see the blue triangle with error bar. All the experimental results are in good agreement with the theoretical results (represented by solid lines) obtained by solving the quantum mechanical dynamics.

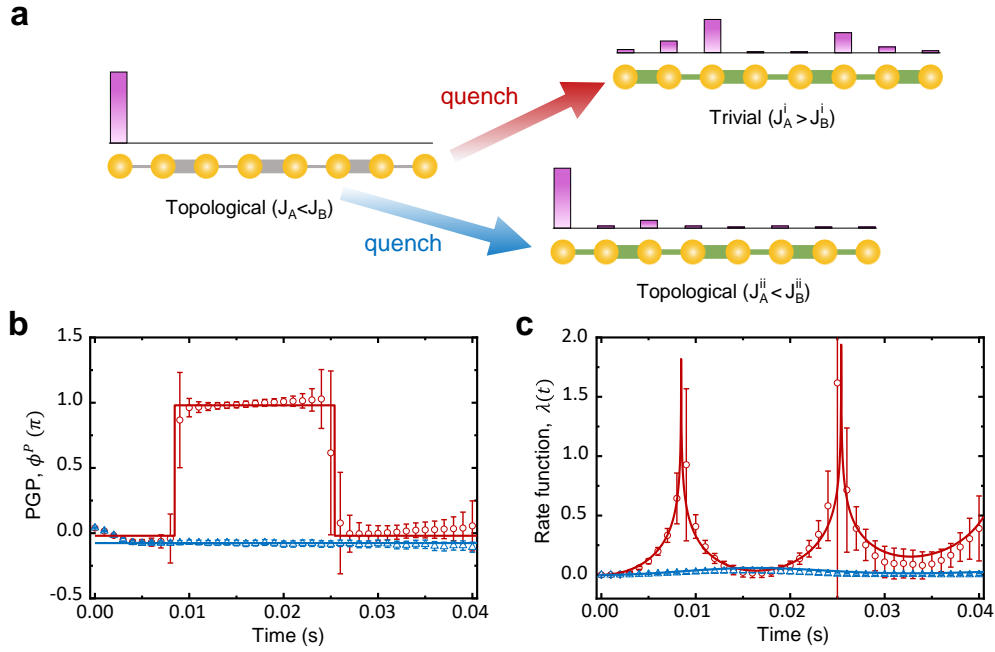


Figure 3: **Dynamical evolution after quench.** **a**, Schematic for the two kinds of sudden quenches in a SSH model with an initial edge state: (i) from topological nontrivial ($J_A < J_B$) to trivial ($J_A^i > J_B^i$) (red arrow), and (ii) from topological nontrivial ($J_A < J_B$) to nontrivial ($J_A^{ii} < J_B^{ii}$) (blue arrow). In the quench-(i), the initial edge state will propagate over the entire chain. In the quench-(ii), the initial edge state will dominate the time-evolution. **b**, The PGP in two different quenches in **a**, which is observed from the demodulating phase of the edge oscillator. The PGP jumps π at each critical time in the quench-(i). The PGP remains unchanged in the quench-(ii). The initial values of PGP are non-zeros constants because of measuring circuit. **c**, The rate function for two different quenches in **a**, which is derived from the normalized amplitude of the edge oscillator, the non-analytic behavior are obvious at DPTs. All solid lines in **b** and **c** are theoretical results derived from quantum mechanics. All error bars denote statistical confidence of one standard deviations.

The two different kinds of quenches can be explained by the partial Loschmidt amplitudes in Fig. 2b and d. Each pair of partial Loschmidt amplitudes with E_{+m} and E_{-m} can be viewed as two vectors rotating around the origin with same length ($|\langle \psi_{\pm m} | \psi(0) \rangle|^2$) and frequency ($|E_{\pm m}|$) but opposite direction. Thus, the summation of all these vector pairs gives a total vector along the real axis, representing the real Loschmidt amplitude. The DPT takes place and PGP jumps π as the Loschmidt amplitude changes between positive and negative. In the sudden quench from topological nontrivial to trivial phases, all pairs of vectors rotate around the origin with non-zero frequencies and so that the total vector can always change direction. In the sudden quench from topological nontrivial to nontrivial phases, the Loschmidt amplitude is dominated by the non-rotating vector pair with zero energy ($|E_{\pm 1}| = 0$) and therefore the total vector will not change its direction.

In summary, by using a reconfigurable nanomechanical array, we directly observe PGP and rate function after a sudden quench from the topological edge state in the SSH model. In the quench from underlying topological nontrivial to trivial phase, we observe π phase jumps of PGP in company with nonanalyticity of rate function, indicating the occurrence of DPTs. In the quench from underlying topological nontrivial to nontrivial phase, we observe that PGP keeps the same while the rate function is analytic. We explore the relation between the PGP and the rate function for diagnosing the dynamical phase transition.

For topological system, there exists bulk-edge correspondence in the equilibrium where the number of edge states corresponds to the bulk topological invariants³⁰. Theoretical results have also shown that the bulk-boundary correspondence for dynamical phase transitions³¹. Experimentally exploring the bulk-edge relations in quenched dynamics will be an interesting and important problem deserving further study. In addition, our system can be used to study more complicated phenomena including interplay between topology, dissipation and nonequilibrium dynamics³².

Methods

The chain coupled oscillators. In our study, eight coupled oscillators are realized by nearest-neighbor parametric couplings. The vibrational amplitudes of the oscillators follow the equations of motion,

$$m_j \ddot{x}_j + m_j \omega_j^2 x_j = L_j(t)(x_{j+1} - x_j) + L_{j-1}(t)(x_{j-1} - x_j) \quad (5)$$

where $L_j(t) = \eta_j \cos[(\omega_{j+1} - \omega_j)t]$ is the time-dependent coupling between the j -th and $(j + 1)$ -th beams. η_j is the coupling strength which can be controlled by the sum of the applied V_{DC} and V_{AC} between the j -th and $(j + 1)$ -th beams. Using slowly varying complex amplitudes ψ_j as $x_j = \sqrt{\hbar\omega_j/(2k_j)} \Re(\psi_j e^{i\omega_j t})$ and rotating wave approximation in Supplementary Information (or see [33,34](#)), the equations of motion can be rewritten as

$$i \frac{\partial}{\partial t} |\psi\rangle = \hat{H} |\psi\rangle \quad (6)$$

where $\psi_j = \langle j | \psi \rangle$ is made to be normalized as $\sum_j |\psi_j|^2 = 1$. H can be made as SSH model by setting $\eta_j \sqrt{\omega_j \omega_{j+1} / k_j k_{j+1}} / 4 = J_A (J_B)$ when $j \in \text{odd}(\text{even})$.

Apart from equation (6), the coherent energy always dissipates into the environment in the actual physics systems. If the decay rate γ_j of each beam is far less than the coupling strength, we can still observe coherent dynamics long before the system decays into the environment. On the other hand, if the beams almost have the same decay rate $\gamma_j = \gamma$ ($j = 1, 2, \dots, 8$), we can separate the complex amplitude as exponential decay term multiple the coherent term, $|\psi\rangle = e^{-\gamma t} |\varphi\rangle$. The dynamics of coherent term $|\varphi\rangle$ is still governed by the SSH model. Based on the two considerations, we try to decrease the decay rates and make a approximation that the decay rates is almost same in short evolution time.

Fabrication of the sample. The sample is fabricated as doubly clamped beams with $200\mu\text{m}$ long on wafers composed of a silicon substrate with 100nm layer of high-stress (1GPa) silicon nitride using the method of low pressure chemical vapor deposition. Electrodes and the wide beam ($3\mu\text{m}$) are defined by standard ultra-violet lithography. All beams and electrodes are thickened by 10nm

Au. The distance between each two adjacent beams is narrowed to 500nm by means of e-beam lithography and ion beam etching (remove metal layer). Reactive ion etching is then employed to eliminate silicon nitride layer. Finally, the mechanical beams are suspended by KOH wet etch. These beams are numbered from 1 to 8. The parameters of the first out-of-plane vibrational mode of every beam in experiments are showed in Table S1.

Parametric Couplings. To generate the electrostatic forces for parametrical couplings between beams, an AC voltage $V_{AC}^j(t)$ and a DC voltage V_{DC} are applied between j -th and $(j + 1)$ -th beam, the coupling as the following form can be generated ²⁸.

$$L_j(t) = \frac{\partial^2 C(\delta x_j)}{\partial^2 \delta x_j} V_{AC}^j(t) V_{DC} \quad (7)$$

Here, $C_j(\delta x_j)$ is the effective capacity between the oscillators and $\delta x_j = x_j - x_{j+1}$. The form of AC voltage is $V_{AC}^j \cos(\omega_{AC}^j t)$ with $\omega_{AC}^j = |\omega_j - \omega_{j+1}|$ and $V_{AC}^j \ll V_{DC}$ in experiment.

The DC voltage and AC voltage are combined by a bias-tee, as showed in Fig. S1 and Fig. S2 where V_P is a sum of the neighborhood AC coupling voltage. The typical value of AC voltage used are listed in Table S2 and Table S3.

The effective coupling strength is confirmed by measuring frequency spectrum of the response. As the Fig. S3 a shows, we measure the response of one oscillator coupled with another adjacent one. The split of peak directly describes coupling strength.

The frequency response of entire coupled chain is measured at edge oscillators, which is showed Fig. S3 c and d, correspond to topological phase and trivial phase of SSH model. Although eight peaks are not distinguishable in these spectrums because of oscillators dissipation, the appearance of zero mode is remarkable distinction between topological and trivial. We also measure the response under the same coupling strengths, showed in Fig. S4.

Measurement Scheme. The sample is placed in a vacuum of 3×10^{-6} Pa and cooled to 77K for the stable frequency and high quality factor. The other measurement circuit at room temperature and all measurements followed the standard magneto-drive method ²⁹. The standard lock-in amplifiers

(The Zurich Instruments HF2LI) are used to measure the frequency-domain spectrums and time-domain measurements. All the frequency generation setups are referencing an external atomic clock to ensure the frequency stability.

It should be pointed out that all of the oscillators work in the linear regime. This can be controlled by the excited strength at the first oscillator. For any oscillator in the linear regime, the relation between the amplitude $|x(\omega)|$ of the vibration and the measured voltage amplitude $|V(\omega)|$ is

$$|x(\omega)| = |V(\omega)|/\xi BL\omega \quad (8)$$

with $\xi \approx 0.83$ the shape factor of the first vibrational mode.

For the parametric coupling, the time-domain measurement is divided into two parts, the diagrams shown in Fig. S1 and Fig. S2. We measure the amplitudes of odd oscillators when the applied coupling voltage V_P and V_{DC} are applied to even oscillators and measure the amplitudes of even oscillators when the applied coupling voltage V_P and V_{DC} are applied to odd oscillators. The amplitude of the first oscillator is monitored to ensure the initial excited strength is the same in both parts. The parameters of the electric circuits and typical coupling voltages are listed in Supplementary Information.

For dynamical measurements, the real-time response of every oscillator is demodulated by fixing its frequency without coupling. All amplitudes measured in the two quenches are shown in Fig. S5, normalized at every moment and shown in Fig. S6 b and d in Supplementary Information.

A sine wave sequence generated by a waveform generator (Keysight 33522B) is an excited source before dynamical quenching. At the same time, the sequence is the reference signal for the lock-in amplifier after quenching when measuring the edge oscillator. In this way, the phase demodulated by the lock-in keeps the same at every measurement and the accuracy of PGP is ensured.

1. Heyl, M., Polkovnikov, A. & Kehrein, S. Dynamical quantum phase transitions in the transverse-field Ising model. *Phys. Rev. Lett.* **110**, 135704 (2013).

2. Heyl, M. Dynamical quantum phase transitions: a review. *Rep. Prog. Phys.* **81**, 054001 (2018).
3. Pancharatnam, S. Generalized theory of interference, and its applications. Part I. Coherent pencils. *Proc. Indian Acad. Sci. Sect. A* **44**, 247-262 (1956).
4. Samuel, J. & Bhandari, R. General setting for berry's phase. *Phys. Rev. Lett.* **60**, 2339-2342 (1988).
5. Budich, J. C. & Heyl, M. Dynamical topological order parameters far from equilibrium. *Phys. Rev. B* **93**, 085416 (2016).
6. Polkovnikov A., Sengupta K., Silva A. & Vengalattore M. Colloquium: Nonequilibrium dynamics of closed interacting quantum systems. *Rev. Mod. Phys.* **83**, 863 (2011)
7. Eisert, J., Friesdorf, M., & Gogolin, C. Quantum many-body systems out of equilibrium. *Nat. Phys.* **11**, 124-130 (2015).
8. Schreiber, M. et al. Observation of many-body localization of interacting fermions in a quasi-random optical lattice. *Science* **349**, 842-845 (2015).
9. Smith, J. et al. Many-body localization in a quantum simulator with programmable random disorder. *Nat. Phys.* **12**, 907-911 (2016).
10. Choi, J.-y. et al. Exploring the many-body localization transition in two dimensions. *Science* **352**, 1547-1552 (2016).
11. Zhang, J. et al. Observation of a discrete time crystal. *Nature* **543**, 217-220 (2017).
12. Choi, S. et al. Observation of discrete time-crystalline order in a disordered dipolar many-body system. *Nature* **543**, 221-225 (2017).
13. Jurcevic, P. et al. Direct observation of dynamical quantum phase transitions in an interacting many-body system. *Phys. Rev. Lett.* **119**, 080501 (2017).

14. Zhang, J. et al. Observation of a many-body dynamical phase transition with a 53-qubit quantum simulator. *Nature* **551**, 601-604 (2017).
15. Bernien, H. et al. Probing many-body dynamics on a 51-atom quantum simulator. *Nature* **551**, 579-584 (2017).
16. Fläschner, N. et al. Observation of dynamical vortices after quenches in a system with topology. *Nat. Phys.* **14**, 265-268 (2018).
17. Wang, C., Zhang, P., Chen, X., Yu, J., & Zhai, H. Scheme to measure the topological number of a Chern insulator from quench dynamics. *Phys. Rev. Lett.* **118**, 185701 (2017).
18. Qiu, X., Deng, T.-S., Guo, G.-C. & Yi, W. Dynamical topological invariants and reduced rate functions for dynamical quantum phase transitions in two dimensions. Preprint at <https://arxiv.org/abs/1804.09032> (2018).
19. Wang, Z., Chong, Y., Joannopoulos, J. D. & Soljačić, M. Observation of unidirectional backscattering-immune topological electromagnetic states. *Nature* **461**, 772775 (2009)
20. Rechtsman, M. C. et al. Photonic Floquet topological insulators. *Nature* **496**, 196-200 (2013).
21. Süsstrunk, R. & Huber, S. D. Observation of phononic helical edge states in a mechanical topological insulator. *Science* **394**, 47-50 (2015).
22. He, C. et al. Acoustic topological insulator and robust one-way sound transport. *Nat. Phys.* **12**, 1124-1129 (2016).
23. St-Jean, P. et al. Lasing in topological edge states of a one-dimensional lattice. *Nat. Photonics* **11**, 651-656 (2017).
24. Su, W. P., Schrieffer, J. R. & Heeger, A. J. Solitons in polyacetylene. *Phys. Rev. Lett.* **42**, 1698-1701 (1979).

25. Asbóth, J. K., Oroszlány, L. & Pályi, A. *A Short Course on Topological Insulators*, vol. 919 of Lecture Notes in Physics (Springer International Publishing, 2016)
26. Sun, W. et al. Uncover topology by quantum quench dynamics. Preprint at <https://arxiv.org/abs/1804.08226> (2017).
27. Huang, P. et al. Nonreciprocal radio frequency transduction in a parametric mechanical artificial lattice. *Phys. Rev. Lett.* **117**, 017701 (2016).
28. Huang, P. et al. Demonstration of motion transduction based on parametrically coupled mechanical resonators. *Phys. Rev. Lett.* **110**, 227202 (2013).
29. Cleland, A. N. & Roukes, M. L. External control of dissipation in a nanometer-scale radiofrequency mechanical resonator. *Sensors and Actuators A* **72**, 256261 (1999).
30. Hatsugai, Y. Chern number and edge states in the integer quantum Hall effect. *Phys. Rev. Lett.* **71**, 3697-3700 (1993).
31. Sedlmayr, N., Jaeger, P., Maiti, M. & Sirker, J. Bulk-boundary correspondence for dynamical phase transitions in one-dimensional topological insulators and superconductors. *Phys. Rev. B* **97**, 064304 (2018).
32. Zhou, L., Wang, Q.-h., Wang, H. & Gong, J. Dynamical quantum phase transitions in non-Hermitian lattices. Preprint at <https://arxiv.org/abs/1711.10741> (2017).
33. Briggs, J. S. & Einfeld, A. Coherent quantum states from classical oscillator amplitudes. *Phys. Rev. A* **85**, 052111 (2012).
34. Briggs, J. S. & Einfeld, A. Quantum dynamics simulation with classical oscillators. *Phys. Rev. A* **88**, 062104 (2013).

Acknowledgements This work was supported by the National Key R&D Program of China (Grant No. 2018YFA0306600), the CAS (Grants No. GJJSTD20170001 and No. QYZDY-SSW-SLH004), and Anhui

Initiative in Quantum Information Technologies (Grant No. AHY050000), and the Natural Science Foundation of China (NNSFC) under Grants No.11574405, 11704420 and 11675163.

Author contributions J.D. and C.L. conceived the project; T.T., L.Z. and P.H. designed the experimental proposal; T.T. and Z.S. prepared the experimental set-up; T.T., L.Z., P.H. and S.L. performed the experiments; S.L. fabricated the sample; Y.K. and T.T. carried out the theoretical calculation; T.T., Y.K. and L.Z. carried out the numerical simulation; all authors contributed to the writing of the manuscript.

Competing Interests The authors declare no competing interests.

Additional information Supplementary information accompanies the paper. Correspondence and requests for materials should be addressed to C.L. (lichao2@mail.sysu.edu.cn) and J.D. (djf@ustc.edu.cn).